RESEARCH ARTICLE

Combine contrast-enhanced 3D T2-weighted short inversion time inversion recovery MR neurography with MR angiography at 1.5 T in the assessment of brachial plexopathy

Zhengdao Xu[1] · Tonghua Zhang[1] · Jianxin Chen[1] · Zongbao Liu[2] · Tao Wang[3] · Yijiang Hu[1] · Jiahui Zhang[1] · Feifei Xue[1]

Abstract

Purpose To explore the benefits of using a single injection of contrast agent at a 1.5 T system to perform both contrast-enhanced MR angiography (MRA) and 3D-T2-STIR MR neurography (MRN) to assess of brachial plexopathy.

Methods In this prospective study, 27 patients with suspected brachial plexopathy, received an imaging procedure composed sequentially of non-enhanced 3D-T2-STIR, CE-MRA, and contrast-enhanced 3D-T2-STIR, using a 1.5 T MR scanner. Signal intensities and contrast ratios were compared with and without contrast agent. The non-enhanced and contrast-enhanced 3D-T2-STIR images were mixed for two experienced radiologists to rate image diagnostic quality in a blind manner. 3D images of MRN and MRA were merged to reveal the spatial relation between brachial plexopathy and concomitant vascular disorders.

Results By comparing the non-enhanced with contrast-enhanced 3D-T2-STIR images, it revealed that the use of the contrast agent in 3D-T2-STIR MRN could significantly suppress the background signals contributed by small vein ($P < 0.001$), lymph node ($P < 0.001$), muscle ($P < 0.001$) and bone ($P < 0.001$). This improved the contrast ratios between the brachial plexus and its surrounding tissues ($P < 0.001$) and boosted the image's quality score ($P < 0.01$). Examining both CE-MRA and 3D-T2-STIR images revealed a relatively high incidence of concurrent vascular dysfunction in brachial plexopathy, with 39% of confirmed cases accompanied with subclavian and axillary vessel abnormalities.

Conclusion Combining contrast-enhanced 3D-T2-STIR MRN with MRA at a 1.5 T system significantly suppresses background signals, improves brachial-plexus display, and provides a direct assessment for both brachial plexus lesion and surrounding vascular injury.

Keywords Brachial plexus · Magnetic resonance neurography · Magnetic resonance angiography · Contrast agent · Brachial plexopathy

---

✉ Zongbao Liu
  liuzongbao1102@163.com

[1] Department of Radiology, The Affiliated Zhangjiagang Hospital of Soochow University, 68 Jiyang West Road, Zhangjiagang 215600, Jiangsu, China

[2] Department of Orthopedics, The Affiliated Zhangjiagang Hospital of Soochow University, 68 Jiyang West Road, Zhangjiagang 215600, Jiangsu, China

[3] Department of Hand Surgery and Shanghai Key Laboratory for Peripheral Nerve and Microsurgery, Fudan University Huashan Hospital, 12 Wulumuqi Middle Road, Shanghai 200040, China

Introduction

The brachial plexus is a network of nerves that extend from the cervical spine to the distal upper limb to provide motor and sensory innervation [1]. Nerve lesions caused by trauma, tumors, inflammation, radiotherapy, or thoracic outlet syndrome often lead to brachial plexopathy, a clinical condition involving upper limb sensory disorders and movement impairments. To characterize the cause and precise location of brachial plexus lesion, several magnetic resonance neurography (MRN) techniques have been applied in the diagnosis of brachial plexopathy [1–5]. Among them, 3D T2-weighted short inversion time inversion recovery (3D-T2-STIR) sequence is the most commonly used [6–9].

With multiplanar and curved planar reconstruction combined with maximum intensity projection (MIP), it can cover the long-extension range of brachial plexus and visualize the entire nerve course from its spinal origin to terminal segments [1, 5]. However, there is one limitation for the conventional 3D-T2-STIR MRN. In addition to nerve fibers showing long-T1 and long-T2 signal characteristics, neighboring tissues such as venules, lymphatic vessels and nodes exhibit similar MR signals, which interfere with the display of brachial plexus and affect diagnosis accuracy. In recent years, some new technologies, such as multi-echo 3D turbo spin-echo modified Dixon (mDixon) sequence and mildly diffusion-weighted sequence, have been developed for MRN to suppress vascular signals surrounding the nerves [10–12], but these methods are more suitable for 3 T systems. Currently, 1.5 T MR scanners are still the most commonly used systems worldwide. Due to the difference in hardware/software, 1.5 T MR scanners are less equipped with the aforementioned sequences. Therefore, for MRN imaging obtained at 1.5 T, reducing the interference from the neighboring tissues to improve the visualization of nerves is an important problem needing research attention. It has recently been reported that applying a contrast agent in 3D-T2-STIR MRN can improve the visibility of peripheral nerves [13–15].

On the other hand, the distribution of brachial plexus is spatially proximate to that of the blood vessel system. The nerves and blood vessels usually accompany each other as they travel through other tissues. Such a close apposition between the brachial plexus and vascular system makes blood vessel dysfunction, one of the major concomitant diseases of brachial plexus neuropathy [16–18]. It has been noted that brachial plexopathy can be associated with arterial/venous injury such as blood vessel rupture, occlusion and compression [19, 20]. Therefore, it is necessary to examine the brachial plexus and its adjacent arteries/veins simultaneously for a comprehensive diagnosis of the disease. In this regard, the conventional 3D-T2-STIR MRN is not able to visualize the neighboring vessels for assessing their involvement in brachial plexopathy.

Based on the above two considerations, we hypothesize that it would be beneficial to use a single injection of contrast agent to carry out both contrast-enhanced 3D-T2-STIR MRN, for better visualization of brachial plexus, and contrast-enhanced (CE) MR angiography (MRA), to reveal surrounding vessels simultaneously. This paper summarizes our studies over the past 3 years and is intended to present a systematic assessment of whether such a combined imaging approach can significantly improve the evaluation of brachial plexopathy with concomitant vascular diseases.

Materials and methods

All patients were informed about imaging procedure details, who signed a written informed consent before the examination. This study was approved by the Human Clinical Research and Ethics Review Board of The First People's Hospital of Zhangjiagang City.

Subjects

This prospective study includes 27 patients with suspected brachial plexopathy (10 men [mean age, 42.3 years; range, 18–69 years] and 17 women [mean age, 45.9 years; range, 22–71 years]; overall age: mean, 44.5 years; range, 18–71 years), who were referred for MR imaging evaluation between December 2014 and December 2017. Clinical history indicated that 9 patients suffered from upper limb numbness, paresthesia, and weakness; 16 had neck and shoulder trauma; 2 had masses in the shoulder. Among all the 27 cases, clinical evaluation, which was based on clinical charts, electrophysiological analyses, and surgical findings, confirmed that 18 patients indeed had brachial plexopathy, while the remaining 9 patients did not show clear evidence for a definitive conclusion. These 18 confirmed cases, which comprised 14 cases of trauma, 2 of tumor and 2 of thoracic outlet syndrome, were all unilaterally affected, with 8 patients on the left side and ten on the right side. The clinical data and imaging findings of confirmed cases are summarised in Supplementary Table 1.

MR imaging

All imaging experiments were performed with a 1.5 T Avanto MR scanner (Siemens Medical System, Erlangen, Germany). A multi-channel head-neck joint coil was combined with a body matrix coil to cover the neck, shoulder and arms. MR images were acquired in the following order, with all acquisition parameters listed in Table 1. Step 1: T1-sequence coronal scanning of 3D volumetric interpolated breath-hold examination (VIBE) to cover the entire brachial plexus on both sides. Step 2: coronal scanning of non-enhanced 3D-T2-STIR used a 3D short inversion time inversion recovery imaging sampling perfection with application optimized contrasts using different flip angle evolutions (3D-STIR SPACE) sequence. Step 3: CE-MRA. A contrast agent, gadopentetic acid dimeglumine salt (Magnevist; Bayer Pharma AG, Berlin, Germany) at a dose of 0.15 mmol/kg, was intravenously injected at a rate of 3.0 ml/s. Right after the emerging of the aortic arch through CARE bolus real-time monitoring, a 3D-FLASH coronal sequence was acquired to reveal the arteries located in the

Table 1 Scanning parameters of the MR pulse sequences used in this study

Parameter	3D-T1-VIBE	3D-STIR SPACE	3D CE-MRA
TR/TE/TI (ms)	7.33/2.39/…	3800/348*/180	3.2/1.18/…
Flip angle (degrees)	10	T2 var**	25
Field of view (mm)	300×300	380×380	360×360
Matrix	256×256	302×320	299×352
Slice thickness (mm)/gap (mm)	1.2/0	1.4/0	1.0/0
Number of slices	104	80	96
Averages	2	1.7	1
Fat suppression	Dixon	STIR	…
GRAPPA acceleration factor	2	3	3
Receiver bandwidth (Hz/pixel)	390	504	490
Turbo factor/Echo spacing (msec)	…	167/4.16	…
Acquisition time (min)	1:51	6:03	0:22

MR magnetic resonance, *TR* repetition time, *TE* time of echo, *TI* inversion time, *GRAPPA* generalized autocalibrating partially parallel acquisition, *VIBE* volumetric interpolated breath hold examination, *SPACE* sampling perfection with application optimized contrasts using different flip angle evolutions, *STIR* short inversion time inversion recovery, *CE-MRA* contrast-enhanced magnetic resonance angiography

*Effective echo time was 108 ms

**The flip angle of the refocusing pulse varies across the echo train. This mode enables very long echo trains for fast T2 weighted measurements and is optimized for specific absorption rate

neck and shoulder region. The 3D-FLASH sequence was repeated immediately after an arterial phase scan to obtain the venous images. Step 4: Contrast-enhanced 3D-T2-STIR scan was performed as in Step 2. Step 5: Contrast-enhanced 3D-T1-VIBE scan was conducted as in Step 1.

Image post-processing and quantitative analysis

Coronal thin-slab MIP reformation was performed using a GE Advantage Workstation (Version 4.5; GE Healthcare, Buc, France), with a 10 mm slice thickness at 3 mm intervals. To compare between the non-enhanced and contrast-enhanced 3D-T2-STIR images, signal intensities of the brachial plexus C7 root and its surrounding tissues, including the C7 vertebra body, scalene muscle, paraspinal vein, and lymph node, were measured by a radiologic technologist (J.Z., with 6-year experience in image post-processing) in the source images of patients' normal healthy sides (Fig. 1). These signal intensities were then compared for each tissue by calculating the ratio of post-versus pre-contrast values in percentage. Further, to evaluate the signal interference of various tissues surrounding the brachial plexus, the contrast ratios between the brachial plexus and other tissues were calculated as follows: $CR = (Signal_{nerve} - Signal_{surrounding\ tissue}) / (Signal_{nerve} + Signal_{surrounding\ tissue})$ [12, 13].

Quality evaluation of MR images

To compare the image diagnostic quality of 3D-T2-STIR scans, the 2 groups of non-enhanced and contrast-enhanced images, including MIP and source formats, were mixed,
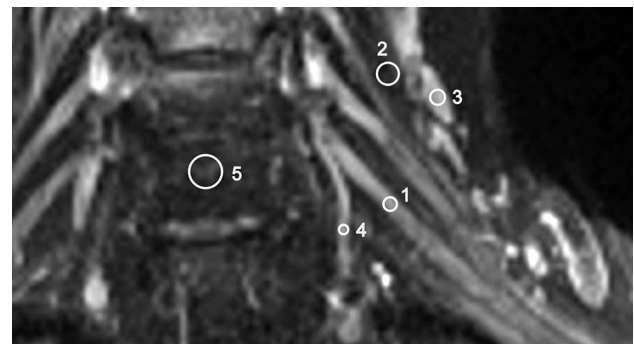

Fig. 1 Representative regions of interest (ROIs) for measuring the signals of the brachial plexus. (1) C7 root, (2) scalene muscle, (3) deep lateral cervical lymph node, (4) paraspinal vein and (5) C7 vertebra body

yielding a random sample pool of 54 image sequences derived from 27 patients. These image sequences were then evaluated by two experienced radiologists (J.C. and T.Z., with 30 and 20 years of experience) in a blind and independent manner, without knowing the imaging acquisition method, electrophysiological finding, previous diagnosis conclusion as well as each other's rating score.

To rate the image diagnostic quality, a three-point grading scale was applied according to the following criteria: 0-point stands for poor nerve visualization, serious interference from surrounding tissues and non-diagnostic; 1-point for moderate nerve visualization, some interference from surrounding tissues but diagnostic; 2-point for

excellent nerve visualization, little interference from other tissues and completely diagnostic [10].

Combining contrast-enhanced MRN with MRA

Previous clinical studies have revealed that a significant proportion of brachial plexopathy cases involving concurrent blood-vessel disorders [18, 20–22], while the diagnostic value of MRN for vascular lesions is relatively limited. This prompted us to review and assess the source and MIP images of CE-MRA for all patients thereby evaluating the concomitant vascular diseases. We merged 3D images of MRA with MRN images using the 3D SynchroView software (GE Healthcare, Buc, France) on the AW4.5 workstation. The software automatically performed the coregistration of MRN and MRA images according to the spatial voxel positioning, then jointly demonstrated the brachial plexus and vascular images. Brachial plexopathy and relevant vascular lesions were observed from different views to reveal their spatial relationship.

Statistical evaluation

Statistical analysis was performed using SPSS 21.0 software (IBM, Chicago, IL, USA). A paired t-test was used to compare various tissues' signal intensities and contrast ratios. Analysis of variance of randomized block design was used to compare the percentage of signals acquired with contrast agent versus without. In case a significant difference was found, a paired t-test with Bonferroni correction was performed for multiple testing. Wilcoxon signed-rank test was applied to compare the three-point grading scores of the non-enhanced and contrast-enhanced images. $P < 0.05$ was considered statistically significant. Kappa inter-observer variability was used to measure the degree of agreement between the two radiologists. $Kappa \leq 0.4$, $0.4 < Kappa < 0.8$, $0.8 \leq Kappa$ were considered, respectively, as poor, good and excellent agreement.

Results

Quantitative analyses of the effects of contrast enhancement

Both contrast-enhanced 3D-T2-STIR MRN and contrast-enhanced MRA were successfully performed in all subjects with a single injection of contrast agent. The brachial plexus was usually not clearly visible in the pre-contrast images, excluding the possibility of tracing the entire nerve course (Fig. 2a). This was largely due to strong background-tissue signals, which severely interfered with the display of brachial plexus. Applying the contrast agent, however, suppressed such background and improved the visibility of brachial plexus dramatically (Fig. 2b).

In the pre-contrast images, the signal intensities for brachial plexus, scalene muscle, lymph node, small vein, and vertebra body were 92.0 ± 20.3, 49.6 ± 8.8, 141.0 ± 27.9, 148.4 ± 39.4, 67.3 ± 16.9, respectively (Fig. 3a, black columns). Applying the contrast agent suppressed the signal levels of all the five tissues (Fig. 3a, grey columns), with their signal intensities reduced to 84.8 ± 18.7, 29.6 ± 6.7, 39.4 ± 16.8, 26.1 ± 10.1, 32.5 ± 9.3, respectively. Comparing these pre- and post-contrast signal intensities revealed
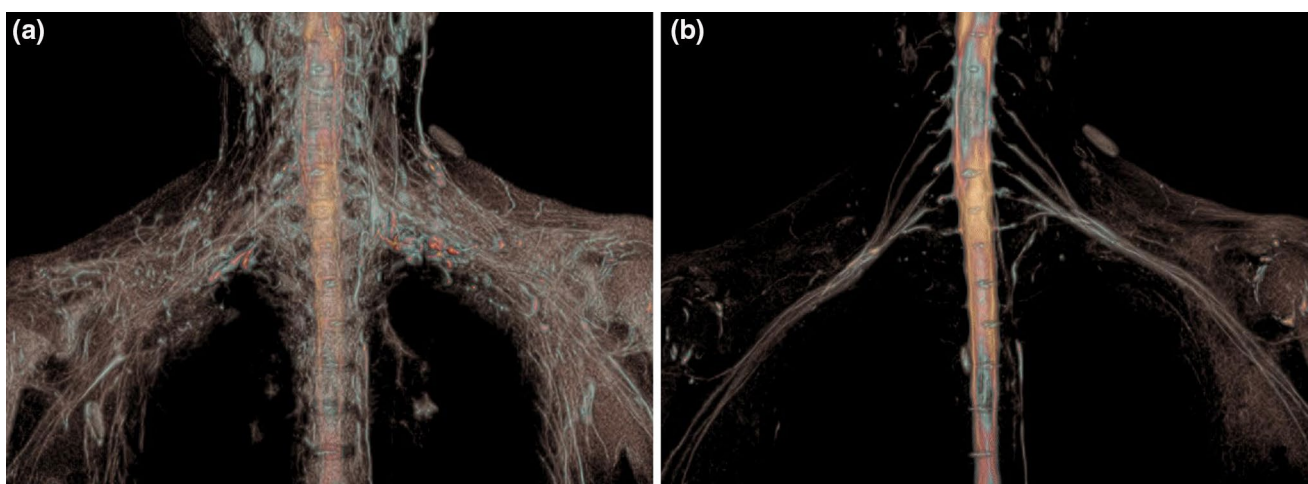

Fig. 2 The effects of applying the contrast agent on 3D-T2-STIR display of the brachial plexus. **a** The pre-contrast volume rendering (VR) image showed poor visualization of brachial plexus. **b** Applying the contrast agent suppressed the signals of the background-tissue, a clear display of brachial plexus was obtained in the post-contrast VR image. This 29-year-old female appeared to have a normal brachial plexus
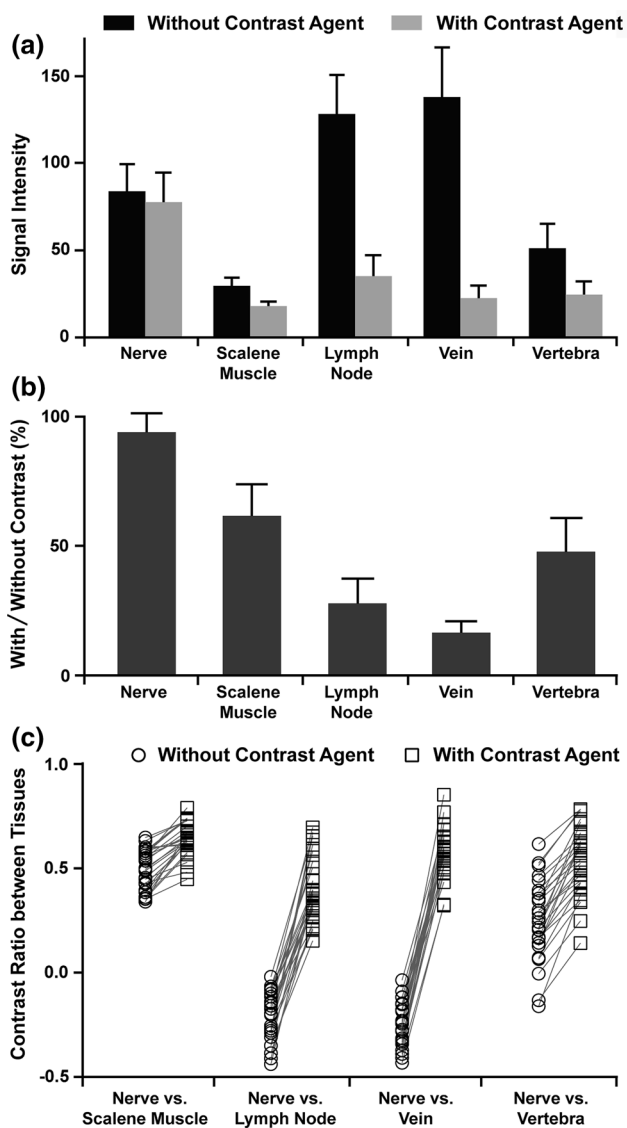
Fig. 3 Quantitative analysis of 3D-T2-STIR images acquired with and without contrast agent. **a** Signal intensity levels of the five tissues before and after injection of the contrast agent, with $P < 0.001$ for all five pairs of comparison. **b** Percentage of signals with versus without contrast agent. The contrast enhancement-induced suppression of the brachial plexus was much less obvious than the suppression of its four surrounding tissues ($P < 0.001$), with the strongest suppression occurring to small vein and lymph node. **c** Changes of contrast ratios between the brachial plexus and the other four tissues in 27 patients. $P < 0.001$ for all four pairs of pre- versus post-contrast comparison

Table 2 Assessment of image diagnostic quality by two independent radiologists

Score	Radiologist #1		Radiologist #2	
	No. of images without CA	No. of images with CA	No. of images without CA	No. of images with CA
0	7	0	4	0
1	18	6	22	4
2	2	21	1	23
Total	27	27	27	27

CA contrast agent

of brachial plexus was significantly lower than those of the other four tissues ($P < 0.001$). As a result, introducing the contrast agent significantly enhanced the contrast ratios between the brachial plexus and its four surrounding tissues (Fig. 3c). The enhancement was from 0.29 ± 0.10 to 0.48 ± 0.11 for scalene muscle, from -0.21 ± 0.13 to 0.39 ± 0.15 for lymph node, from -0.22 ± 0.15 to 0.53 ± 0.14 for small vein, and from 0.15 ± 0.16 to 0.44 ± 0.14 for vertebra ($P < 0.001$ for all four comparisons). It should be noted that the nerve-to-vein and nerve-to-lymph contrast ratios exhibited an even more dramatic increase, as revealed by the much steeper slope between each patient's pre- and post-contrast data points in Fig. 3c.

Image diagnostic quality evaluation

The results of the image diagnostic quality analysis for all patients are shown in Table 2. The diagnostic quality scores in images with contrast agent (the median of the score was 2 in both readers) were significantly ($P < 0.01$) higher than those in images without contrast agent (the median of the score was 1 in both readers), as reported by both readers. By introducing a contrast agent, the image diagnostic quality scores from both radiologists significantly improved. For inter-observer agreement, Kappa values for images with and without contrast agent were 0.514 and 0.465, respectively. Applying the contrast agent revealed brachial plexus and its lesions more clearly in the 3D-T2-STIR MRN (Figs. 4 and 5).

Combining contrast-enhanced MRN with MRA

The presence of vascular dysfunction was frequently observed in patients with traumatic brachial plexus injury. Of the 14 traumatic cases we examined, 6 patients showed abnormality either in the subclavian or axillary artery in CE-MRA images. Moreover, brachial plexus-related tumors potentially affected peripheral blood vessels. In one patient, we revealed the subclavian vein invasion and
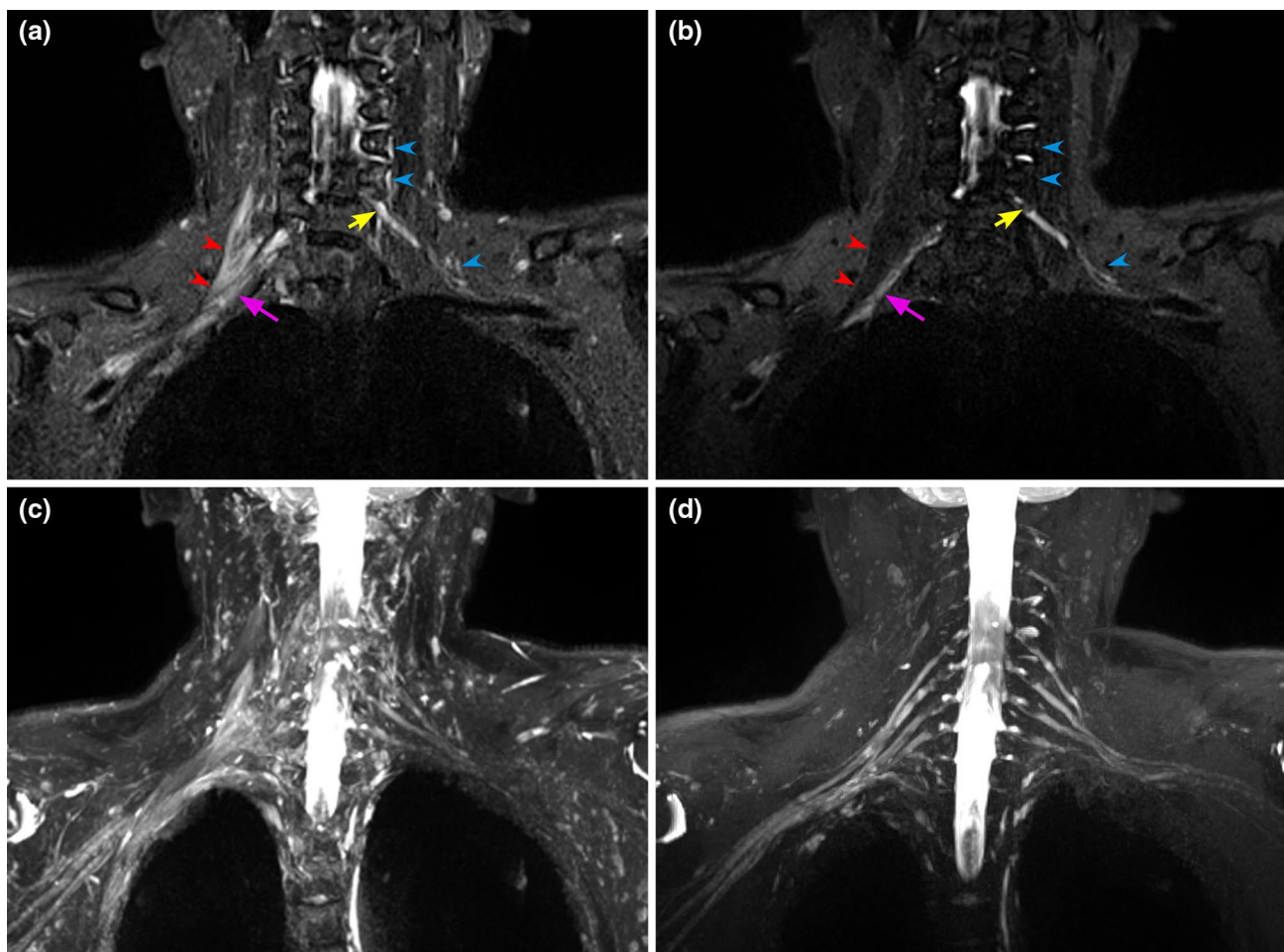
statistically significant differences, with $P < 0.001$ for all the five tissues. The signals of small veins and lymph nodes were found to be suppressed the most dramatically, with only 15.3% and 26.7% of their pre-contrast signal remained (Fig. 3b). The vertebra and muscle retained 46.7% and 60.5% of pre-contrast signals. On the other hand, the suppressing effect on the brachial plexus was quite small, with 92.9% of signal remained. Therefore, the signal suppression

Fig. 4 A 44-year-old male with a right-neck trauma 10 days before imaging. **a** The swollen right-side scalene muscle (red arrowheads), small veins (blue arrowheads), displayed high signals similar to the nerves in the pre-contrast source image. **b** The high signals from the scalene muscle and veins were completely suppressed in the post-contrast source image, and the middle trunk of the right brachial plexus (pink arrow) could be distinguished clearly. **c** In the pre-con-trast MIP image, the strong background signals obscured the display of brachial plexus. **d** Contrast enhancement suppressed these signals and significantly improved nerve delineation in the post-contrast MIP image, revealing the swelling and inhomogeneity of the upper and middle trunks and cords of the right brachial plexus. The small black spot of brachial plexus root displayed in (**b**) is the spinal ganglion (yellow arrow)

occlusion by metastatic tumors. These visible vascular lesions in CE-MRA images were all clinically confirmed in our study. Combining MRN with MRA provided a more complete picture of the relationship between nerve lesions and vascular diseases (Figs. 6 and 7), which was essential for guiding subsequent treatments.

Overall, of the 18 clinical confirmed cases of brachial plexopathy, 7 patients showed concomitant subclavian and axillary vessel abnormalities, reaching an incidence rate of 39%. This highlights the necessity of combining MRN and MRA with a single injection of the contrast agent for the diagnosis of brachial plexopathy.

Discussion

In this study, we demonstrate that contrast-enhanced images of the brachial plexus with background suppression and images of adjacent vessels can be obtained simultaneously after a single injection of contrast agent at a 1.5 T system. Moreover, brachial plexopathy and vascular injury could be evaluated in parallel.

Compared with 1.5 T, 3 T systems are highly preferred for MRN imaging. A few newer types of sequences have been developed for MRN at 3 T systems recently.
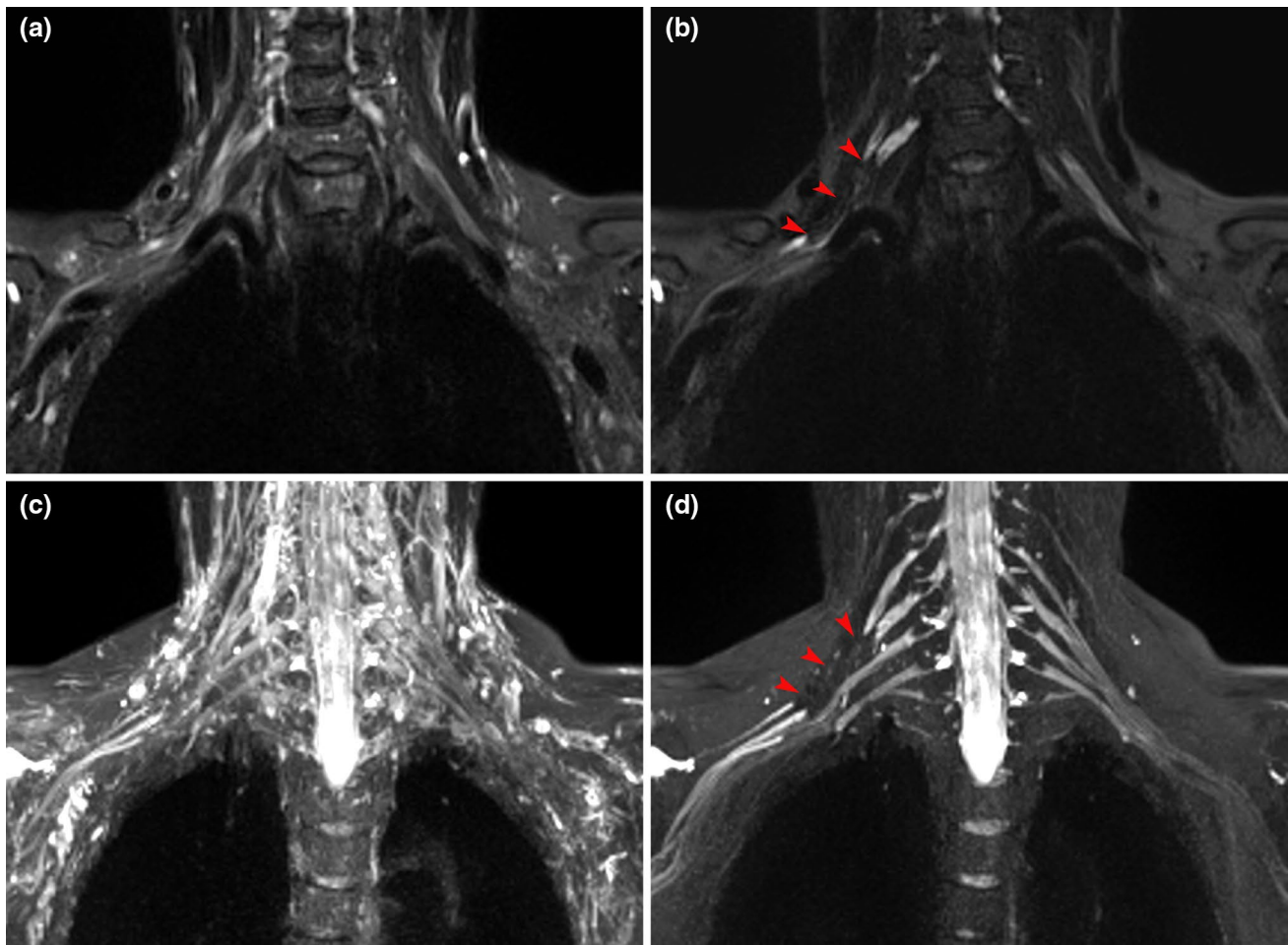
Fig. 5 A 60-year-old female with a history of breast cancer resection suffered from the numbness of her right upper limb and limited mobility for 4 months. **a** The lesions in the right upper trunk of the brachial plexus were not shown clearly in the pre-contrast source image. **b** The post-contrast source image displayed a decreased signal in the local area of the upper trunk (red arrowhead). **c** The pre-contrast MIP image had a poor visualization of the brachial plexus and its lesions. **d** The post-contrast MIP image, however, demonstrated a filling defect area in the right upper trunk (red arrowhead), which was presumably caused by a damage in the blood-nerve barrier due to tumor invasion. This was confirmed by postoperative pathology revealing that metastatic adenocarcinoma invaded the brachial plexus

Multi-echo 3D turbo spin-echo mDixon sequence, which integrates multi-echo chemical shift acquisitions with a modified 3D TSE flip angle train, provides robust fat and blood suppression [10]. 3D nerve-sheath signal increased with inked rest-tissue rapid acquisition of relaxation imaging (3D SHINKEI) is also a new sequence that suppresses signals from blood vessels, muscles, and fat tissue using improved motion-sensitized driven equilibrium (iMSDE) and spectral attenuated inversion recovery [23, 24]. These novel methods can effectively suppress background-tissue signals, in particular, to reduce the interference of neighboring veins during nerve observation. Therefore, the new 3 T MR scanner is the top-notch equipment for MRN imaging currently.

However, The 1.5 T MR scanners are still the most widely used MR systems worldwide. Due to hardware and software limitations, the sequences mentioned above rarely can be applied to the 1.5 T MR scanner. The conventional MRN yields low image quality on the 1.5 T MR scanner compared with the 3 T, but the 1.5 T MR scanner has the advantages of lower specific absorption rate and fewer artifacts. In this study, we used the 3D-T2-STIR sequence for MRN after intravenous injection of contrast agent to the 1.5 T system. The contrast-enhanced 3D-T2-STIR MRN images provide better contrast ratios between nerve and surrounding tissues compared with non-enhanced images. As an essential quantitative imaging parameter, it was reported that the comparisons based on contrast ratios concur well with subjective visual evaluation, and the increased contrast ratios could improve the diagnostic ability [14]. Our subjective evaluation also confirmed that the quality of post-contrast images was better than that of pre-contrast images. Besides,
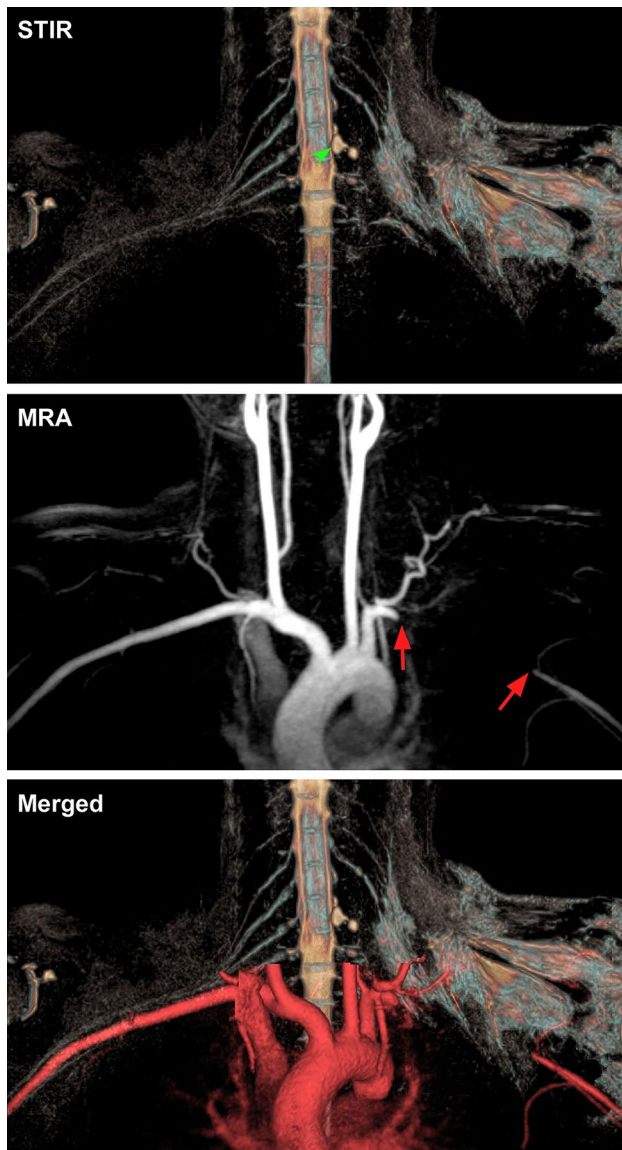
Fig. 6 A 25-year-old male with brachial-plexus nerve root avulsion and subclavian artery damage in the left shoulder. The images were taken 14 days after a motorcycle accident. Contrast-enhanced 3D-T2-STIR neurograph revealed neurotmesis in the C6-T1 roots of the left brachial plexus as well as formation of traumatic pseudomeningocele (as indicated by a green arrowhead in upper panel). There was widespread soft tissue edema over the left shoulder. Two red arrows in the contrast-enhanced MR angiograph (middle panel) indicate the damage and occlusion of the left subclavian artery. The display of the downstream axillary artery, which appeared to be much thinner than the axillary artery on the opposite side, was due to contrast agent entering through collateral circulation. The neurograph and angiograph were combined in the lower panel to show their spatial relationship

benefiting from the 3D acquisition, the axial, coronal, sagittal, and oblique images can be reconstructed from source images of the contrast-enhanced 3D-T2-STIR sequence, facilitating the evaluation of brachial plexopathy.
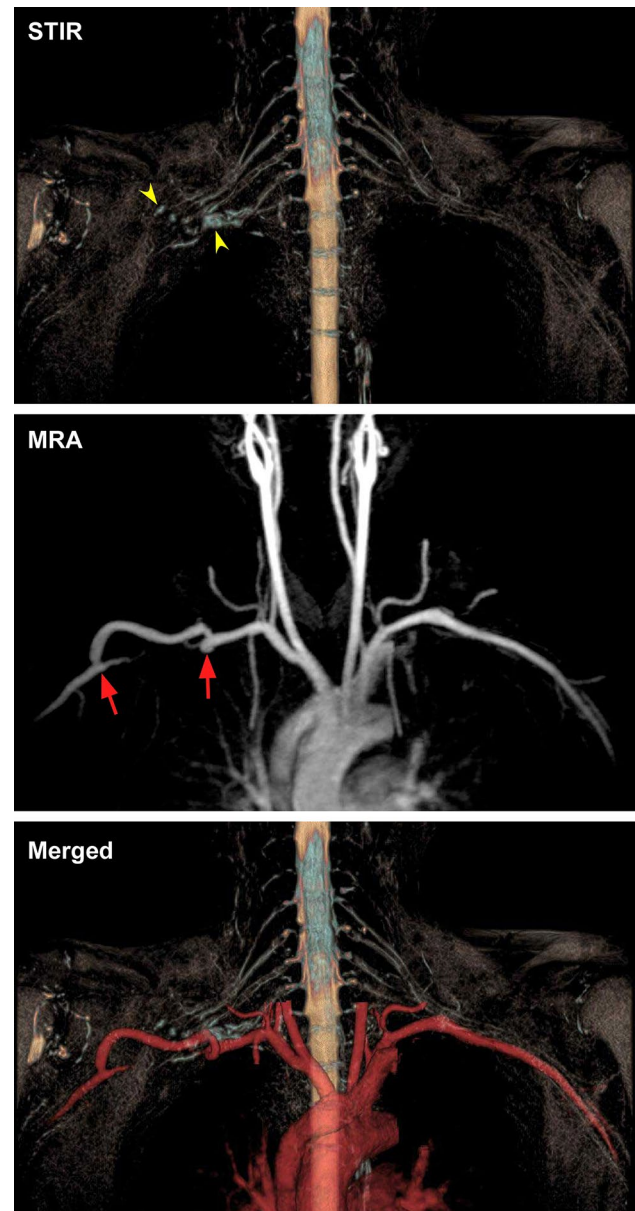

Fig. 7 A 53-year-old male with brachial-plexus neurotmesis who had an axillary artery-bypass surgery about 1 year before imaging. Upper panel, a contrast-enhanced 3D-T2-STIR neurograph demonstrated neurotmesis in the upper, middle and lower trunks of the right brachial plexus, with small neuromata (yellow arrowheads) developed locally in these trunks. Middle panel, a contrast-enhanced MR angiograph revealed that an artery-bypass graft was made to the right axillary artery between the locations as indicated by two red arrows. Lower panel, the neurograph and angiograph were merged to visualize the spatial relationship between the graft vessel and the sites of brachial plexus injury

The brachial plexus and some of its surrounding tissues, like small veins, venules, lymphatic vessels, and nodes, are characterized by a long T1 and long T2 relaxation time and thus display high signals in the conventional non-enhanced 3D-T2-STIR images. Small veins and lymph nodes have an

even much higher signal level than the brachial plexus, and this explains why the conventional 3D-T2-STIR MRN usually has a strong background that obscures the nerves display. Our direct comparison between the non-enhanced and contrast-enhanced 3D-T2-STIR images reveals that the paramagnetic contrast agent can significantly improve the display of peripheral nerves by suppressing background-tissue signals, which is consistent with previous studies [13–15]. Among several factors, the STIR inversion pulse of the 3D-T2-STIR sequence appears to be one major contributor to this improvement. STIR sequence is originally designed for fat suppression by taking advantage of fat tissue's short T1 relaxation time. When other non-fat background tissues (such as small veins and lymph nodes) absorb the contrast agent, their T1 relaxation time is shortened to be similar to that of fat tissue [25]. With an inversion time of 180 ms used in our 3D-T2-STIR sequence, the STIR pulse can non-selectively suppress the signals from these background tissues [26]. Meanwhile, the contrast agents also shorten the T2 relaxation time of the above tissues [25], while the TE of the 3D-T2-STIR sequence is long, with image characteristics of the T2-weighted sequence; thus, background signals could be further decreased.

The nerve tissue, on the contrary, absorbs little contrast agent [27] and thus has a very limited T1 and T2 shortening effect. Consequently, the brachial plexus can retain relatively high signal of its pre-contrast level, whereas the signals for small veins and lymph nodes are sharply reduced. Such a differential shortening of relaxation time presents a mechanism for increasing the contrast ratios between nerves and surrounding tissues to improve the image's diagnostic quality. In the case of trauma, the injury-induced swollen muscles also absorb more contrast agent, and its high signal would be suppressed in the post-contrast images to avoid interference to the nerves.

One exception for peripheral nerves is the spinal ganglion, where there is abundant blood circulation. The relatively high absorption of contrast agent turns a ganglion into a dark breaking point along the otherwise continuous bright nerve trajectory [13]. On the other hand, if a contrast-enhanced 3D-T2-STIR image reveals a nerve-darkening area at a non-ganglion location, it is very likely that the nerve at this location is injured. The damaged blood-nerve barrier allows the entry of the contrast agent [27, 28], which induce signals suppression from the injured nerve. This may presumably be called "*The Negative Contrast Enhancement Effect*". In this regard, an unusual darkening area along the nerve course can be an indicator of nerve lesion.

The brachial plexus is divided into five parts from proximal to distal end, including the roots, trunks, divisions, cords, and branches. Among them, the division and cord nerves run closely with the subclavian and axillary vessels [29]. Any factors causing brachial plexopathy, such as trauma and tumors, would also likely lead to concurrent blood-vessel disorders [21, 22, 30, 31]. Under such a situation, the diagnosis of the vascular lesion can be easily overlooked by clinical examination due to collateral circulation compensation. However, such a vascular lesion alters blood supply in the affected upper limb, which can have adverse effects on the recovery and regeneration of injured brachial-plexus nerves. Furthermore, if not treated timely, the site of vascular damage can develop pseudoaneurysm, which would compress the brachial plexus and cause additional pathological changes [32]. Therefore, in the case of brachial plexopathy involving trauma, tumor, and thoracic outlet syndrome, it is essential to use CE-MRA to detect the injury, stenosis, occlusion, and compression of adjacent blood vessels [16, 18, 33, 34]. The 3D volume-rendering display of merged vascular and neural images can reveal the anatomical relationship between brachial plexopathy and adjacent vascular lesion, which may provide critical information for selecting appropriate treatment regimens; and guiding surgical operation and determining the prognosis of the disease.

Kappa values represent the degree of agreement between observers. When the Kappa values approach to 1, the agreement between the two observers is considered better. In this study, we obtained Kappa values for images with and without contrast agent as 0.514 and 0.465, respectively. Such Kappa values were considered good rather than excellent, and this may be ascribed to a small overall sample size. When the sample size is small, even a few cases of inconsistency in the scores graded by the two readers decrease the Kappa values significantly. In this study, the number of cases in which two readers graded different scores to the images with and without contrast agent was 4 and 6, respectively. In the cases with different scores, the difference-value between the scores of the two readers was 1 point, and none of the cases had a difference-value of 2 points, implying a relatively small difference in scores. Besides, the gap between the two readers' work experience was 10 years, and the difference in diagnosis experience might explain the discrepancy in scores between them.

One potential drawback for the contrast-enhanced 3D-T2-STIR MRN is related to the neoplastic lesion of brachial plexus. Tumor growth is often associated with angiogenesis, which brings in a rich supply of blood. This may lead to the suppression of tumor signals and thereby affect tumor detection. Therefore, we included the 3D-T1-VIBE sequence in our study to reveal the enhancement of tumor efficiently. Another problem is that 3D fusion of angiograph and neurograph requires a patient to remain in the same body position without movement throughout the entire imaging session. Otherwise, anatomical dislocation and mismatch can occur in the merged image. The five-step imaging procedure employed in this study generally took about 20 min, which can be difficult for those patients experiencing pain.

The major time-consuming scans are the two 3D-T2-STIR sequences taken with and without contrast agent, with each scan lasting over 6 min. To shorten the imaging session, the non-enhanced 3D-T2-STIR scan can be omitted, especially for non-tumor patients. Due to the small sample size, we only included confirmed cases of brachial plexopathy with trauma, tumor, and thoracic outlet syndrome. Contrast-enhanced 3D-T2-STIR MRN might be most suitable for these lesions. A limitation of this study is the lack of evaluation for other types of brachial plexopathy, such as radiation-induced changes, idiopathic brachial neuritis, and chronic inflammatory demyelinating polyneuropathy. Therefore, follow-up studies should be directed to these types of lesions. The safety issues associated with gadolinium-based contrast agents such as nephrogenic systemic fibrosis, gadolinium deposition, also require in-depth attention. In the future, we intend to use safer macrocyclic gadolinium-based contrast agents such as gadobutrol instead of Magnevist (a linear gadolinium-based contrast agent) for imaging.

In summary, the contrast-enhanced 3D-T2-STIR sequence can selectively suppress background-tissue signals, and thereby significantly improve an image's diagnostic quality. Combining contrast-enhanced neurography with angiography at a 1.5 T MR scanner for simultaneous display of the brachial plexus and adjacent vessels is a viable procedure for the diagnosis and assessment of both brachial plexus lesions and any surrounding vascular injury. With further optimization of scan parameters, this combined imaging approach will have broad applications in the clinical examination of peripheral neuropathy.

Compliance with ethical standards

References

1. Vargas MI, Viallon M, Nguyen D, Beaulieu JY, Delavelle J, Becker M (2010) New approaches in imaging of the brachial plexus. Eur J Radiol 74:403–410. https://doi.org/10.1016/j.ejrad.2010.01.024

2. Vargas MI, Gariani J, Delattre BA, Dietemann JL, Lovblad K, Becker M (2015) Three-dimensional MR imaging of the brachial plexus. Semin Musculoskelet Radiol 19:137–148. https://doi.org/10.1055/s-0035-1546300

3. Lutz AM, Gold G, Beaulieu C (2014) MR imaging of the brachial plexus. Neuroimaging Clin N Am 24:91–108. https://doi.org/10.1016/j.nic.2013.03.024

4. Madhuranthakam AJ, Lenkinski RE (2015) Technical advancements in MR neurography. Semin Musculoskelet Radiol 19:86–93. https://doi.org/10.1055/s-0035-1547370

5. Chhabra A, Thawait GK, Soldatos T, Thakkar RS, Del GF, Chalian M et al (2013) High-resolution 3T MR neurography of the brachial plexus and its branches, with emphasis on 3D imaging. AJNR Am J Neuroradiol 34:486–497. https://doi.org/10.3174/ajnr.A3287

6. Viallon M, Vargas MI, Jlassi H, Lovblad KO, Delavelle J (2008) High-resolution and functional magnetic resonance imaging of the brachial plexus using an isotropic 3D T2 STIR (Short Term Inversion Recovery) SPACE sequence and diffusion tensor imaging. Eur Radiol 18:1018–1023. https://doi.org/10.1007/s00330-007-0834-4

7. Upadhyaya V, Upadhyaya DN, Kumar A, Gujral RB (2015) MR neurography in traumatic brachial plexopathy. Eur J Radiol 84:927–932. https://doi.org/10.1016/j.ejrad.2015.02.006

8. Baumer P, Kele H, Kretschmer T, Koenig R, Pedro M, Bendszus M et al (2014) Thoracic outlet syndrome in 3T MR neurography-fibrous bands causing discernible lesions of the lower brachial plexus. Eur Radiol 24:756–761. https://doi.org/10.1007/s00330-013-3060-2

9. Chhabra A, Carrino J (2015) Current MR neurography techniques and whole-body MR neurography. Semin Musculoskelet Radiol 19:79–85. https://doi.org/10.1055/s-0035-1545074

10. Wang X, Harrison C, Mariappan YK, Gopalakrishnan K, Chhabra A, Lenkinski RE et al (2017) MR neurography of brachial plexus at 3.0 T with robust fat and blood suppression. Radiology 283:538–546. https://doi.org/10.1148/radiol.2016152842

11. Klupp E, Cervantes B, Sollmann N, Treibel F, Weidlich D, Baum T et al (2019) Improved brachial plexus visualization using an adiabatic iMSDE-prepared STIR 3D TSE. Clin Neuroradiol 29:631–638. https://doi.org/10.1007/s00062-018-0706-0

12. Yoneyama M, Takahara T, Kwee TC, Nakamura M, Tabuchi T (2013) Rapid high resolution MR neurography with a diffusion-weighted pre-pulse. Magn Reson Med Sci 12:111–119. https://doi.org/10.2463/mrms.2012-0063

13. Chen WC, Tsai YH, Weng HH, Wang SC, Liu HL, Peng SL et al (2014) Value of enhancement technique in 3D–T2-STIR images of the brachial plexus. J Comput Assist Tomogr 38:335–339. https://doi.org/10.1097/RCT.0000000000000061

14. Wang L, Niu Y, Kong X, Yu Q, Kong X, Lv Y et al (2016) The application of paramagnetic contrast-based T2 effect to 3D heavily T2W high-resolution MR imaging of the brachial plexus and its branches. Eur J Radiol 85:578–584. https://doi.org/10.1016/j.ejrad.2015.12.001

15. Zhang X, Li M, Guan J, Wang H, Li S, Guo Y et al (2017) Evaluation of the sacral nerve plexus in pelvic endometriosis by three-dimensional MR neurography. J Magn Reson Imaging 45:1225–1231. https://doi.org/10.1002/jmri.25435

16. Aralasmak A, Karaali K, Cevikol C, Uysal H, Senol U (2010) MR imaging findings in brachial plexopathy with thoracic outlet

syndrome. AJNR Am J Neuroradiol 31:410–417. https://doi.org/10.3174/ajnr.A1700

17. Verenna AA, Alexandru D, Karimi A, Brown JM, Bove GM, Daly FJ et al (2016) Dorsal Scapular Artery Variations and Relationship to the Brachial Plexus, and a Related Thoracic Outlet Syndrome Case. J Brachial Plex Peripher Nerve Inj 11:e21–e28. https://doi.org/10.1055/s-0036-1583756

18. Aralasmak A, Cevikol C, Karaali K, Senol U, Sharifov R, Kilicarslan R et al (2012) MRI findings in thoracic outlet syndrome. Skeletal Radiol 41:1365–1374. https://doi.org/10.1007/s00256-012-1485-3

19. Zarkadas PC, Throckmorton TW, Steinmann SP (2008) Neurovascular injuries in shoulder trauma. Orthop Clin North Am 39:483–490. https://doi.org/10.1016/j.ocl.2008.06.005

20. Araujo JD, Azenha Filho JO, Barros ET, Marconi A (1988) Reciprocal compression between the axillary artery and brachial plexus. J Cardiovasc Surg 29:172

21. Johnson SF, Johnson SB, Strodel WE, Barker DE, Kearney PA (1991) Brachial plexus injury: association with subclavian and axillary vascular trauma. J Trauma 31:1546–1550

22. Rasulic L, Savic A, Lepic M, Puzovic V, Karaleic S, Kovacevic V et al (2018) Epidemiological characteristics of surgically treated civilian traumatic brachial plexus injuries in Serbia. Acta Neurochir (Wien) 160:1837–1845. https://doi.org/10.1007/s00701-018-3640-7

23. Kasper JM, Wadhwa V, Scott KM, Rozen S, Xi Y, Chhabra A (2015) SHINKEI–a novel 3D isotropic MR neurography technique: technical advantages over 3DIRTSE-based imaging. Eur Radiol 25:1672–1677. https://doi.org/10.1007/s00330-014-3552-8

24. Hiwatashi A, Togao O, Yamashita K, Kikuchi K, Ogata H, Yamasaki R et al (2017) Evaluation of chronic inflammatory demyelinating polyneuropathy: 3D nerve-sheath signal increased with inked rest-tissue rapid acquisition of relaxation enhancement imaging (3D SHINKEI). Eur Radiol 27:447–453. https://doi.org/10.1007/s00330-016-4406-3

25. Weinmann HJ, Brasch RC, Press WR, Wesbey GE (1984) Characteristics of gadolinium-DTPA complex: a potential NMR contrast agent. AJR Am J Roentgenol 142:619–624. https://doi.org/10.2214/ajr.142.3.619

26. Krinsky G, Rofsky NM, Weinreb JC (1996) Nonspecificity of short inversion time inversion recovery (STIR) as a technique of fat suppression: pitfalls in image interpretation. AJR Am J Roentgenol 166:523–526. https://doi.org/10.2214/ajr.166.3.8623620

27. Kobayashi S, Meir A, Baba H, Uchida K, Hayakawa K (2005) Imaging of intraneural edema by using gadolinium-enhanced MR imaging: experimental compression injury. AJNR Am J Neuroradiol 26:973–980

28. Hill BJ, Padgett KR, Kalra V, Marcillo A, Bowen B, Pattany P et al (2018) Gadolinium DTPA enhancement characteristics of the rat sciatic nerve after crush injury at 4.7T. AJNR Am J Neuroradiol 39:177–183. https://doi.org/10.3174/ajnr.A5437

29. Bowen BC, Pattany PM, Saraf-Lavi E, Maravilla KR (2004) The brachial plexus: normal anatomy, pathology, and MR imaging. Neuroimaging Clin N Am 14:59–85. https://doi.org/10.1016/j.nic.2003.12.002

30. Binder DK, Smith JS, Barbaro NM (2004) Primary brachial plexus tumors: imaging, surgical, and pathological findings in 25 patients. Neurosurg Focus 16:E11

31. Qayyum A, MacVicar AD, Padhani AR, Revell P, Husband JE (2000) Symptomatic brachial plexopathy following treatment for breast cancer: utility of MR imaging with surface-coil techniques. Radiology 214:837–842. https://doi.org/10.1148/radiology.214.3.r00mr11837

32. Chen L, Peng F, Wang T, Chen D, Yang J (2014) Traumatic pseudoaneurysm of axillary artery combined with brachial plexus injury. PLoS ONE 9:e113099. https://doi.org/10.1371/journal.pone.0113099

33. Charon JP, Milne W, Sheppard DG, Houston JG (2004) Evaluation of MR angiographic technique in the assessment of thoracic outlet syndrome. Clin Radiol 59:588–595. https://doi.org/10.1016/j.crad.2003.11.020

34. Ersoy H, Steigner ML, Coyner KB, Gerhard-Herman MD, Rybicki FJ, Bueno R et al (2012) Vascular thoracic outlet syndrome: protocol design and diagnostic value of contrast-enhanced 3D MR angiography and equilibrium phase imaging on 1.5- and 3-T MRI scanners. AJR Am J Roentgenol 198:1180–1187. https://doi.org/10.2214/AJR.11.6417